

2B-300:

Using CALIOP Retrieved Aerosol Parameters to Improve OCO-2 Version 8 Retrievals

Aronne Merrelli*

Space Science and Engineering Center (SSEC), University of Wisconsin–Madison

Ralf Bennartz

Vanderbilt University, Dept. of Earth & Environmental Sciences
Space Science and Engineering Center (SSEC), University of Wisconsin–Madison

Chris O'Dell, Tommy Taylor, Heather Cronk

Cooperative Institute for Research in the Atmosphere (CIRA), Colorado State University

1. INTRODUCTION

The NASA Orbiting Carbon Observatory-2 (OCO-2) mission is designed to retrieve the dry air column integrated mole fraction of carbon dioxide (X_{CO_2}) at sufficiently high accuracy to allow estimation of surface CO_2 fluxes at regional scales (Crisp 2015). Since the launch of OCO-2 in 2014, the instrument has shown excellent accuracy and precision for L1b radiance products (Crisp 2017). For the L2 X_{CO_2} retrieval product, operational bias correction and filtering methods yield a global X_{CO_2} dataset with an uncertainty estimated to be 0.4 ppm, when compared to co-located TCCON measurements (Wunch 2017). On a smaller spatial scale, there are known correlated errors (or equivalently, regional biases) that are possibly related to aerosol or surface property modeling in the L2 retrieval.

In this study, we attempt to reduce some of the apparent bias in the L2 retrieval due to aerosol modeling by utilizing data from the CALIOP LIDAR instrument aboard the CALIPSO spacecraft. OCO-2 and CALIPSO are both in the NASA A-Train instrument formation, and since August 2015 the two spacecraft have flown in a tight formation that aligns the LIDAR footprint inside OCO-2's swath. The resulting spatial footprints match to within 4 km at the surface.

Customized data files containing CALIOP L2 layer retrieval data co-located to OCO-2 footprints are routinely processed at CIRA's Data Processing Center, along with various MODIS-Aqua cloud and imagery products. These data products have proven useful in validation of OCO-2

cloud screening validation (Taylor 2016). Recent reprocessing of the data has included the version 4 CALIOP aerosol layer retrievals, which contain various improvements in aerosol detection and optical depth retrieval (Kim 2018).

The general approach in this study is to use CALIOP's knowledge of the aerosol presence and vertical placement as prior information for the OCO-2 L2 retrieval. For this initial study, only cloud free scenes are selected. Cloud screening is performed by limiting the analysis to orbits where the operational OCO-2 cloud screening mask, the CALIOP vertical feature mask, and RGB imagery from the Aqua MODIS instrument all indicate large regions of cloud free atmosphere. Note the OCO-2 cloud screening methods will also remove thicker aerosol layers, as the screening methods are sensitive to scattering particle layers of any type (see Taylor 2016 for details). We assume that any thin aerosol layers present in the data after screening are spatially homogeneous. In section 2, we briefly review the OCO-2 L2 algorithm and our modifications to include the CALIOP layer data. The OCO-2 data subset and TCCON comparison data are described in section 3, followed by analysis procedures in section 4. Our results are shown in section 5, followed by conclusions in section 6.

2. RETRIEVAL ALGORITHM

The operational OCO-2 L2 algorithm (known as the ACOS algorithm) is fully described by the L2 Algorithm Theoretical Basis Document (ATBD) and O'Dell 2018. Briefly, the algorithm is a standard optimal estimation (OE) approach applied to a physical forward model to compute radiances

* Corresponding author address: SSEC, Univ. of Wisconsin–Madison, 1225 W. Dayton Street, Madison, WI, 53706; e-mail: aronne.merrelli@ssec.wisc.edu

at the OCO-2 spectral sampling grids. The forward model, for the current Build 8 (B8) version of ACOS, includes 5 scattering particles: water cloud, ice cloud, stratospheric aerosol, and two tropospheric aerosols selected from a MERRA climatology. All aerosols have a Gaussian vertical profile for concentration (ρ), using the following equation,

$$\rho(x) = C \exp\left(-\frac{(x - x_0)^2}{2\sigma^2}\right)$$

where x is the pressure relative to the surface pressure (scaled pressure height), and σ is the scaled pressure width. The constant C is set such that the total vertical integral is equal to the required aerosol optical depth (AOD) at 755 nm, and the logarithm of the AOD is included in the state vector. The constant x_0 is the scaled pressure level for the center of the aerosol layer. All aerosols have fixed pressure widths and the stratospheric aerosol has a fixed pressure height ($x_0 = 0.006$). The remaining nine parameters: OD for the five particles, and pressure heights for both MERRA aerosols and cloud types, are unconstrained by the OE prior. Thus, a simple way to utilize the CALIOP derived aerosol information is to set different prior means and uncertainties for these nine parameters according to the CALIOP layer data.

2.1 MODIFIED RETRIEVAL ALGORITHM: CALIOP-DERIVED PRIORS

The CALIOP retrieval produces a highly accurate vertical position of the aerosol layer. However, the extinction optical depth of the aerosol layer has higher uncertainty, due to assumptions about aerosol types via the Lidar ratio (Kim 2018, Oo 2011). To translate the optical depth values to OCO-2, an aerosol optical depth from CALIOP would need to be converted into an extinction optical depth at 755 nm, which would incur additional uncertainty. For clouds, the Lidar ratio has much less variability, and thus the CALIOP cloud optical depth has relatively less uncertainty. Finally, the detection limit of CALIOP must be considered. A “clear scene” as defined by the CALIOP retrieval may still have thin undetected aerosol layers, especially since we are using the daytime observations where scattered solar radiation degrades the LIDAR’s signal to noise ratio. Our prior constraint values for OCO-2 retrievals must therefore allow for relatively thin aerosol layers to be included in the forward model, rather than simply removing the aerosols completely from the state vector.

The translation of the CALIOP layer data into a prior for the OCO-2 retrieval algorithm is a partially subjective process, guided by intuition. The general characteristics of the CALIOP retrieval suggests that the layer height information should be used as a tight constraint for ACOS, while the AOD should be a relatively loose constraint. The cloud optical depth constraint should be intermediate, since the CALIOP cloud optical depth should be more accurate. For cases where the CALIOP retrieval does not detect a cloud or aerosol layer, we use a prior value for OD that is much lower than the ACOS B8 but leave the prior uncertainty relatively large (factor of 4). This allows the ACOS algorithm to fit thin aerosol layers ($\tau < 0.03$) that are likely undetected by CALIOP (Kim 2017). Table 1 summarizes the prior mean and (1- σ) standard deviation for each of these variables. Note that the uncertainty ranges for the optical depths are multiplicative (e.g., ± 6 implies that 1-sigma range is a multiplicative factor of 6).

Parameter	B8 Oper. Prior	Modified value (CALIOP clear)	Modified value (CALIOP detection)
OD mean			
Water Cld	0.0125	0.002	CALIOP L2 layer OD
Ice Cld	0.0125	0.002	
Trop. Aer	MERRA	0.002	
x_0 mean			
Water Cld	0.75	0.75	CALIOP L2 layer P/Ps
Ice Cld	tropopause	0.3	
Trop. Aer	0.9	0.9	
OD uncert.			
Water Cld	± 6	± 1.5	± 1.5
Ice Cld	± 6	± 1.5	± 1.5
Trop. Aer	± 7.4	± 4	± 5
x_0 uncert.			
Water Cld	± 0.4	± 0.4	± 0.005
Ice Cld	± 0.2	± 0.05	± 0.005
Trop. Aer	± 0.2	± 0.2	± 0.005

Table 1. Summary of Aerosol and cloud related state vector variables used in the ACOS retrieval, for the B8 operational algorithm, and the modified version using CALIOP clear, and CALIOP layer detections.

After adjusting the prior aerosol information, the operational algorithm was rerun over sets of OCO-2 soundings, described in section 3. Other than the adjustment to the aerosol prior, the modified algorithm is identical to the B8 operational algorithm.

3. DATASETS

3.1 OCO-2 SOUNDINGS

OCO-2 orbit tracks were selected through two geographical regions: the Eastern Saharan desert and the central plains region of the US. The first region was chosen for this study due to the relatively high fraction of cloud free, aerosol affected scenes. For these cases, cloud free scenes were selected from OCO-2 Nadir observation geometry that crossed with a latitude and longitude box covering the Eastern Sahara (17.5° – 32.5° latitude, 10° – 35° longitude). To limit the total amount of data, orbits were included from every third month between December 2015 and ending in March 2017. A total of 53 orbits were selected. The second region was chosen to allow for comparison to the TCCON station at Lamont, Oklahoma. For these cases, the matchup requires a part of the OCO-2 Nadir track to pass within $\pm 6^\circ$ longitude of the TCCON site, similar to matchup criteria of TCCON – OCO-2 in previous studies (O'Dell 2018, Wunch 2017). A total of 48 OCO-2 orbits were selected from this data group from August 2015 to October 2017. To limit the total amount of sounding data, only the subsets of soundings within $\pm 1^\circ$ latitude of Lamont are included. The resulting matchup region is 12° in longitude and 2° in latitude, centered on Lamont.

For each of the identified passes, the OCO-2 soundings that appear in the spatial selection window are further divided into “small areas”. Following O'Dell 2018, the orbit segment is first subdivided into blocks of spatially contiguous soundings. Each block is recursively divided in half, until the blocks have no more than 50 frames. At the typical spacing of OCO-2 soundings (each frame of 8 soundings is separated by approximately 2.3 km along track), this yields a spatial area of approximately 100 km along track. Within this small area, in the absence of strong CO₂ point sources (such as power plants), the true spatial variability of X_{CO2} is much smaller than the single sounding uncertainty. For example, the spatial variability estimated from simulated X_{CO2} fields is smaller than 0.1 ppm on 100 km spatial scales (Worden 2017). Therefore, we compute simple statistics (mean and standard deviation) over the group of soundings within each small area in order to evaluate the retrieval output. A typical small area will have several hundred soundings (50 frames with 8 soundings each, minus those soundings rejected

by the various filtration steps), and a minimum of 30 soundings, as small areas with fewer soundings are discarded. The standard deviation over these soundings is an empirical estimate of the true scatter in the retrieved X_{CO2}. Figure 1 shows an example from each region, where the mapped points are colored according to the small area subdivisions. The small area subdivision yields a total of 416 small areas in the Sahara group, and 129 small areas in the Lamont group.

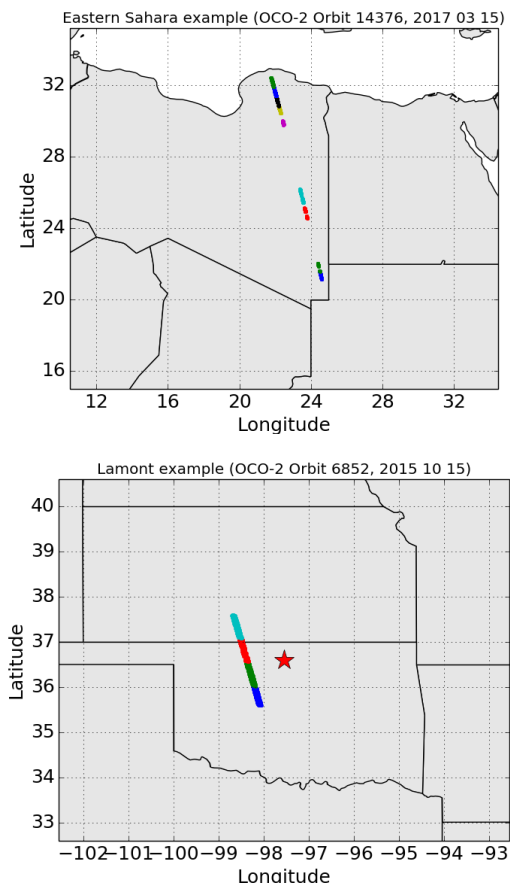


Figure 1. Example OCO-2 ground tracks used in the study, colored according to small area subgroupings: Eastern Sahara region (top) and central US plains (bottom). The position of the Lamont TCCON site is marked with a red star.

3.2 TCCON DATA

The Lamont TCCON data was accessed from the TCCON website (Wennberg 2017). The TCCON retrieval produces hundreds of daytime X_{CO2} samples, limited to clear sky conditions. Using a matchup window period of 2 hours before and after the OCO-2 overpass time, each day contains roughly 50 TCCON samples. These are averaged

to a single TCCON comparison value for each OCO-2 orbit in the data sample.

4. ANALYSIS

To evaluate the modified retrieval output, we compare X_{CO_2} and two variables used in X_{CO_2} bias correction: “delta surface pressure”, and “co2 grad del”. The first variable (called “dP” in short form) is the difference between the retrieved surface pressure and the prior surface pressure from Numerical Weather Prediction analysis fields (O’Dell 2018). The second variable, “co2_grad_del” is the difference between the retrieved and prior values of the vertical gradient of the CO_2 concentration profile. The vertical gradient is approximated with the finite difference between the CO_2 concentration at the surface and at 0.7 times the surface pressure. Both variables have been used for bias correction in ACOS applied to OCO-2 soundings and GOSAT soundings (Wunch 2011, O’Dell 2018, OCO-2 ATDB, 2017).

For the X_{CO_2} analysis, we consider the raw X_{CO_2} and two versions of bias corrected X_{CO_2} . The linear bias correction for X_{CO_2} is derived from analysis of global OCO-2 data compared to several “truth proxy” datasets for X_{CO_2} (O’Dell 2018). The bias correction process reduces both bias (e.g., the mean difference between the retrieved X_{CO_2} and the truth proxy) and scatter (the standard deviation of the X_{CO_2} differences). We do not necessarily expect the bias correction derived for the Version 8 ACOS algorithm to be optimal for the modified algorithm. It is likely that the operational bias correction is mitigating the impact of aerosol modeling errors to some extent, and our modified algorithm has important changes to the algorithm’s treatment of aerosol. However, developing a bias correction scheme requires a much larger amount of data, including global coverage and spanning the widest possible range of scene conditions. We cannot derive a similar correction for our modified algorithm using the standard approach, because there is not sufficient data.

Due to these limitations, we apply a modified, “partial” bias correction that applies only the global scaling factor and the footprint-dependent bias correction. These two components of the bias correction are likely present in the modified algorithm output in a similar way as the operational ACOS algorithm output. This partial bias correction does not include the parametric terms (dP, co2_grad_del, and an aerosol optical

depth variable; see O’Dell 2018, L2 ATBD). Finally, the full operational B8 bias correction is applied to both datasets, while acknowledging that the results for the modified algorithm may not be optimal.

5. RESULTS

After performing the various processing described in the previous section, we have mean and standard deviation values for the 5 variables (dP, co2_grad_del, raw and two bias corrected X_{CO_2}) in each small area. In each case, we compute the same values from the operational B8 retrieval output from the same soundings. In all cases we only examine the subset of soundings that are deemed “good quality” according to the B8 data quality assessment (See O’Dell 2018).

Since the modified algorithm impacts the aerosol retrieval, the analysis is aided by defining a new variable that is the ratio between the total AOD in the modified retrieval and the total AOD in the operational retrieval. Values greater than unity indicate that the modified algorithm retrieved more AOD (in the small area average), and less than unity indicates less AOD in the small area average. Generally, values less than unity correspond to small areas where the CALIOP did not detect an aerosol layer, so the tendency is for the modified prior to suppress the total AOD.

Figure 2 shows a scatter plot of the difference in dP (left column) and co2_grad_del (right column) between the modified and operational algorithm results. The top row contains the differences in the small area mean values, and the bottom row contains the differences in small area standard deviation values. Results for the East Saharan region are shown in orange, and the near Lamont region results are shown in blue. The dP difference in mean shows a clear correlation to the AOD ratio. The modified algorithm shows a higher dP bias when the retrieved AOD is lower than operational, and lower dP bias when the retrieved AOD is higher than normal. The dP bias is also lower at a ratio of unity, indicating that the modification will tend to reduce dP even if the AOD does not change – in which case the aerosol height prior change is causing the differences. Retrievals from both regions show similar patterns, however the quantitative distributions are slightly different. For the dP standard deviation, we see a tendency for reduced scatter in dP with lower AOD, and increased scatter for higher AOD. The

co2_grad_del shows weaker correlation, but with a reversed correlation sign for the difference in mean.

Figure 3 shows the raw X_{CO_2} (left column) and full bias corrected X_{CO_2} (right column), displayed with similar coordinates to Figure 2. The partial bias correction results are not shown. For the partial bias correction, the primary change is the global scaling factor, which affects both results equally, and therefore there is no significant change in the differences. For X_{CO_2} , there is larger separation between the results from the two data regions, primarily in the mean raw X_{CO_2} (upper left). The scatter in raw X_{CO_2} shows the clearest evidence of improvement in the modified retrieval. Recall that for these small areas, the scatter (as estimated by the standard deviation) will be driven almost entirely by uncertainty in the retrieval, not real signatures in the X_{CO_2} field. In the lower left panel, the raw X_{CO_2} scatter is reduced by approximately 0 – 0.5 ppm for cases where the modified algorithm retrieves less AOD. For the reverse case (more AOD in modified retrieval), the scatter increases, with some extreme values (up to +2 ppm) for the largest AOD increase. After bias correction, this improvement disappears. The difference between the bias corrected X_{CO_2} is nearly uncorrelated with the AOD ratio, and centered on zero (meaning, no change in X_{CO_2} scatter).

Finally, for the Lamont dataset, we can compare the TCCON and OCO-2 X_{CO_2} values. For each OCO-2 orbit, each small area produces a mean X_{CO_2} value, and these multiple values are compared to the single TCCON mean value for the overpass time. There may be additional true variation in the X_{CO_2} field between small areas, which we cannot estimate. However, this additional variation will impact both the operational algorithm and the modified algorithm, so it should not change the relative comparison between the two algorithms. Figure 4 shows scatter plots and summary statistics for the OCO-2 – TCCON results. The left column shows the operational results, and the right column shows the modified algorithm results, where the rows show the comparison with raw OCO-2 X_{CO_2} (top), partial bias corrected OCO-2 X_{CO_2} (middle), and full bias corrected OCO-2 X_{CO_2} (bottom). Each subplot shows the correlation coefficient, and the standard deviation and bias (the mean value) of the OCO-2 – TCCON differences. All variants of X_{CO_2} from the modified algorithm show an increase in bias magnitude of 0.3 ppm compared to the operational algorithm. The modified algorithm shows an approximately 20%

reduction in scatter in raw ΔX_{CO_2} and in partial bias corrected raw ΔX_{CO_2} (from 1.2 to 1 ppm). For the full bias correction, both algorithms show identical scatter (0.95 ppm).

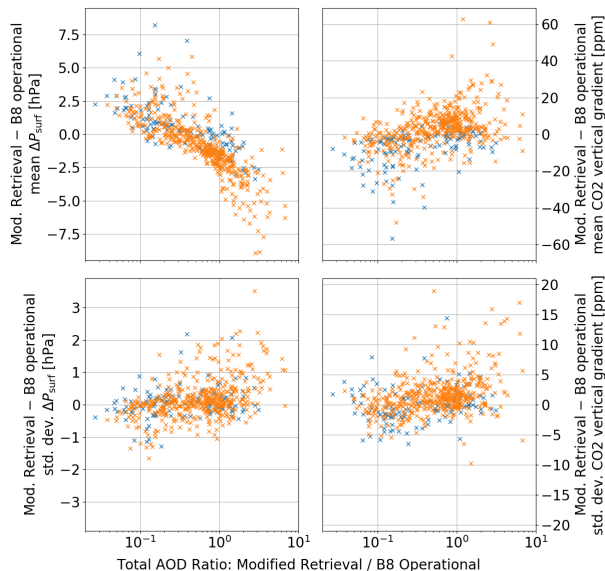


Figure 2. Results for dP and $co2_grad_del$ from Sahara (Orange) and Lamont (Blue), plotted versus AOD ratio.

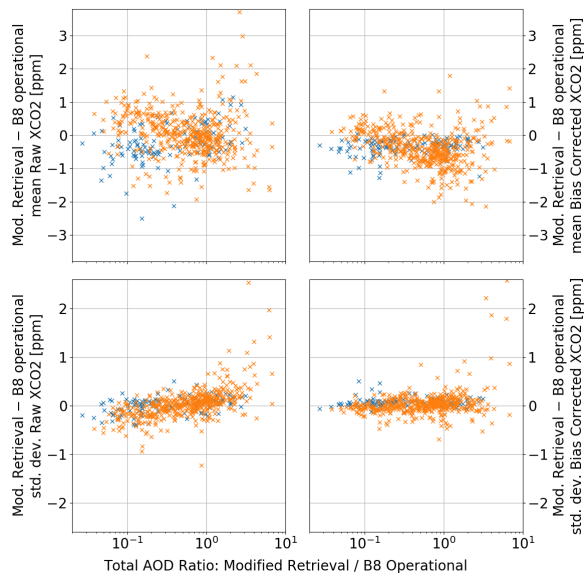


Figure 3. Results for raw X_{CO_2} and bias corrected X_{CO_2} , plotted analogously to Figure 2.

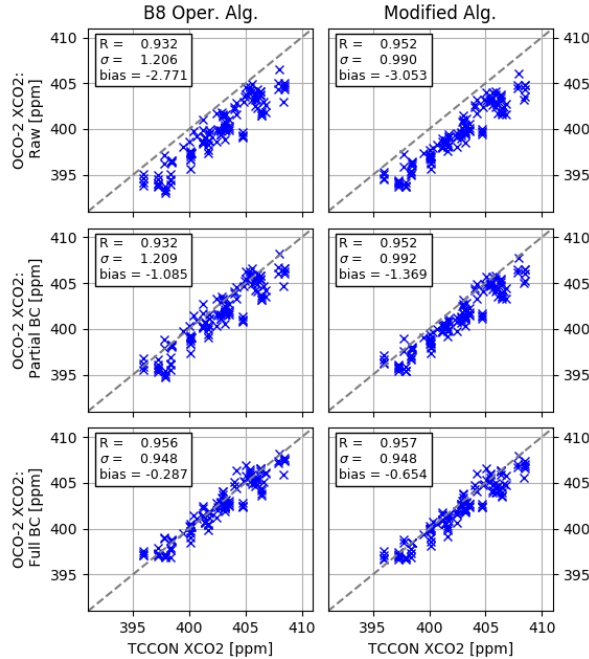


Figure 4. Comparison of Operational Algorithm (left) and Modified Algorithm (right) to TCCON. Rows show different X_{CO_2} values: raw (top), partial bias corrected (middle), and full bias correction (bottom).

6. CONCLUSIONS

This study evaluated a simple method of applying CALIOP aerosol retrieval information to OCO-2 algorithms with the aim of improving the X_{CO_2} retrieval. Overall, the raw X_{CO_2} shows reduced scatter in small area statistics, but only when the modified retrieval has less AOD than the operational retrieval. After the full bias correction, the two algorithms show equivalent X_{CO_2} scatter. Note that the modified algorithm's X_{CO_2} does show similar scatter to the full bias corrected, operational X_{CO_2} (0.99 compared to 0.95 ppm). The modified algorithm shows an increased absolute X_{CO_2} bias of 0.36 ppm relative to the Lamont TCCON.

The results do not support a general conclusion that CALIOP data will not improve X_{CO_2} retrievals using ACOS. If additional analysis can produce an optimal bias correction for the modified algorithm, it may compare more favorably to the operational algorithm. In addition, the results do suggest that a more sophisticated approach than aerosol prior modification should be explored. Additional research is needed to explore alternative methods. Here we summarize various limitations of the presented approach, and suggest further research that could better utilize CALIOP data to improve X_{CO_2} retrieval:

1) The presented approach relies on CALIOP L2 aerosol layer retrievals. This introduces undesirable artifacts in the ACOS retrievals near the spatial edges of the CALIOP aerosol layer. For example, at the edges of each CALIOP layer feature (which will have a horizontal length of 5, 20, or 80 km depending on the spatial averaging applied to the Level 1B CALIOP data – see CALIOP L2 ATBD), there will be neighboring soundings that have very different priors (see Table 1). In addition, this translation would not be effective for any cases with multiple vertical layers, since the single aggregated CALIOP layer and single Gaussian profile used by the ACOS retrieval need to be reasonable approximations of the true aerosol vertical profile.

2) No attempt has been made to utilize the CALIOP aerosol type information, due to the uncertainty of translating the CALIOP retrieved AOD at 532 nm to OCO-2 AOD referenced to 755 nm. A more accurate approach may need to use consistent aerosol scattering properties across both the CALIOP L2 layer retrieval algorithms and the ACOS algorithm.

3) CALIOP's sensitivity may not be high enough to give useful information for most of the clear scenes used in the operational OCO-2 retrievals. A recent study with CALIOP (Kim 2017) suggests total aerosol optical depth up to approximately 0.1 could be undetected in the ascending (daytime) passes, due to the detector noise and increased background from scattered solar radiation. The majority of OCO-2 good quality soundings are below AOD 0.1.

These limitations could be addressed more directly by a joint retrieval that utilizes a combined measurement vector including OCO-2 radiance spectra and a co-located CALIOP backscatter profile. The joint retrieval would avoid the nonlinearity associated with the detection or non-detection of an aerosol layer, and allow more realistic vertical profiles. The aerosol scattering properties would be directly shared between each forward model. Finally, the lower sensitivity of CALIOP could be handled more consistently, as the retrieval would be able to fit thin aerosol layers that would still be consistent with the sensitivity of the backscatter profiles.

Acknowledgements. This research was partially supported by NASA grant NNX15AH96G, awarded through the Research Opportunities in Earth and Space Science program.

7. REFERENCES

CALIOP L2 Feature Detection and Layer Properties Algorithms ATBD, available at NASA LARC: https://www-calipso.larc.nasa.gov/resources/project_documentation.php

Crisp, D. 2015: Measuring atmospheric carbon dioxide from space with the Orbiting Carbon Observatory-2 (OCO-2), *Earth Observing Systems XX, Proceedings of SPIE*, 9607, 960702.

Crisp, D. et al., 2017: The on-orbit performance of the Orbiting Carbon Observatory-2 (OCO-2) instrument and its radiometrically calibrated products. *Atm. Meas. Tech.*, 10, 59-81.

Eldering, A. et al., 2017: The Orbiting Carbon Observatory-2: first 18 months of science data products. *Atm. Meas. Tech.*, 10, 549-563.

Kim, M. H. et al., 2018: The CALIPSO Version 4 Automated Aerosol Classification and Lidar Ratio Selection Algorithm. In review at *Atm. Meas. Tech. Discussions*, doi: 10.5194/amt-2018-166.

Kim, M. H. et al., 2017: Quantifying the low bias of CALIPSO's column aerosol optical depth due to undetected aerosol layers. *J. Geophys. Res.: Atm.*, 122, 1098-1113.

OCO-2 Algorithm Theoretical Basis Document (L2 ATBD) for Data Release 8 (2017). available at NASA GES DISC: <https://disc.gsfc.nasa.gov/information/documents?title=OCO-2%20Documents>

O'Dell, C. W. et al., 2018: *Retrievals of Carbon Dioxide from the Orbiting Carbon Observatory-2 with the ACOS algorithm*. Submitted to *Atm. Meas. Tech.*

Oo, M. and Holz, R. E., 2011: Improving the CALIOP aerosol optical depth using combined MODIS-CALIOP observations and CALIOP integrated attenuated total color ratio. *J. Geophys. Res.: Atm.*, 116, D14201.

Taylor, T. et al., 2016: Orbiting Carbon Observatory-2 (OCO-2) cloud screening algorithms: validation against collocated MODIS and CALIOP data. *Atm. Meas. Tech.*, 9, 973-989.

Wennberg, P., et al.: TCCON data from Lamont, Oklahoma, USA, Release GGG2014R0. Last accessed 2017. <http://dx.doi.org/10.14291/tcon.ggg2014.lamont01.R0/1149159>

Worden, J. R. et al., 2017: Evaluation and attribution of OCO-2 X_{CO_2} uncertainties. *Atm. Meas. Tech.* 10, 2759-2771.

Wunch, D. et al., 2011: A method for evaluating bias in global measurements of CO₂ total columns from space. *Atm. Chem. Phys.*, 11, 12317-12337.

Wunch, D. et al., 2017: Comparisons of the Orbiting Carbon Observatory-2 (OCO-2) X_{CO_2} measurements with TCCON., *Atm. Meas. Tech.*, 10, 2209-2238.